Tunable fractional-order photonic differentiator based on the inverse Raman scattering in a silicon microring resonator

Boyuan Jin,[1] Jinhui Yuan,[1,2,*] Chongxiu Yu,[1] Xinzhu Sang,[1] Qiang Wu,[1,3] Feng Li,[2] Kuiru Wang,[1] Binbin Yan,[1] Gerald Farrell[4], and P. K. A. Wai[2]

[1] *State Key Laboratory of Information Photonics and Optical Communications, Beijing University of Posts and Telecommunications, Beijing 100876, China*

[2] *Photonics Research Centre, Department of Electronic and Information Engineering, The Hong Kong Polytechnic University, Hung Hom, Kowloon, Hong Kong*

[3] *Department of Physics and Electrical Engineering, Northumbria University, Newcastle upon Tyne, NE1 8ST, United Kingdom*

[4] *Photonics Research Center, School of Electronic and Communications Engineering, Dublin Institute of Technology, Kevin Street, Dublin 8, Ireland*

[*] *yuanjinhui81@163.com*

Abstract: A novel photonic fractional-order temporal differentiator is proposed based on the inverse Raman scattering (IRS) in the side-coupled silicon microring resonator. By controlling the power of the pump light-wave, the intracavity loss is adjusted and the coupling state of the microring resonator can be changed, so the continuously tunable differentiation order is achieved. The influences of input pulse width on the differentiation order and the output deviation are discussed. Due to the narrow bandwidth of IRS in silicon, the intracavity loss can be adjusted on a specific resonance while keeping the adjacent resonances undisturbed. It can be expected that the proposed scheme has the potential to realize different differentiation orders simultaneously at different resonant wavelengths.

OCIS codes: (200.4740) Optical processing; (130.3120) Integrated optics devices; (190.5650) Raman effect; (320.5540) Pulse shaping.

References and links

1. F. Li, Y. Park, and J. Azaña, "Complete temporal pulse characterization based on phase reconstruction using optical ultrafast differentiation (PROUD)," Opt. Lett. **32**(22), 3364–3366 (2007).
2. J. Yao, F. Zeng, and Q. Wang, "Photonic generation of ultra-wideband signals," J. Lightwave Technol. **25**(11), 3219–3235 (2007).
3. Y. Park, M. Kulishov, R. Slavík, and J. Azaña, "Picosecond and sub-picosecond flat-top pulse generation using uniform long-period fiber gratings," Opt. Express **14**(26), 12670–12678 (2006).
4. J. Silva and M. Campos, "Spectrally efficient UWB pulse shaping with application in orthogonal PSM," IEEE Trans. Commun. **55**(2), 313–322 (2007).
5. N. Ngo, S. Yu, S. Tjin, and C. Kam, "A new theoretical basis of higher-derivative optical differentiators," Opt. Commun. **230**(1-3), 115–129 (2004).
6. R. Slavík, Y. Park, M. Kulishov, and J. Azaña, "Terahertz-bandwidth high-order temporal differentiators based on phase-shifted long-period fiber gratings," Opt. Lett. **34**(20), 3116–3118 (2009).
7. J. Dong, A. Zheng, Y. Zhang, J. Xia, S. Tan, T. Yang, and X. Zhang, "Photonic Hilbert transformer employing on-chip photonic crystal nanocavity," J. Lightwave Technol. **32**(20), 3704–3709 (2014).
8. W. Zhang, W. Li, and J. Yao, "Optical differentiator based on an integrated sidewall phase-shifted Bragg grating," IEEE Photon. Technol. Lett. **26**(23), 2383–2386 (2014).
9. H. Zhang, M. Tang, Y. Xie, S. Fu, D. Liu, and P. P. Shum, "Programmable wavelength-tunable second-order optical temporal differentiator based on a linearly chirped fiber Bragg grating and a digital thermal controller," Opt. Lett. **39**(7), 2004–2007 (2014).
10. J. Dong, Y. Yu, Y. Zhang, B. Luo, T. Yang, and X. Zhang, "Arbitrary-order bandwidth-tunable temporal differentiator using a programmable optical pulse shaper," IEEE Photon. J. **3**(6), 996–1003 (2011).
11. J. Dong, A. Zheng, D. Gao, L. Lei, D. Huang, and X. Zhang, "Compact, flexible and versatile photonic differentiator using silicon Mach-Zehnder interferometers," Opt. Express **21**(6), 7014–7024 (2013).
12. J. Dong, A. Zheng, D. Gao, S. Liao, L. Lei, D. Huang, and X. Zhang, "High-order photonic differentiator employing on-chip cascaded microring resonators," Opt. Lett. **38**(5), 628–630 (2013).

#233705 - $15.00 USD Received 3 Feb 2015; revised 15 Apr 2015; accepted 16 Apr 2015; published 21 Apr 2015

13. Y. Hu, L. Zhang, X. Xiao, Z. Li, Y. Li, T. Chu, Y. Su, Y. Yu, and J. Yu, "An ultra-high-speed photonic temporal differentiator using cascaded SOI microring resonators," J. Opt. **14**(6), 065501 (2012).
14. F. Liu, T. Wang, L. Qiang, T. Ye, Z. Zhang, M. Qiu, and Y. Su, "Compact optical temporal differentiator based on silicon microring resonator," Opt. Express **16**(20), 15880–15886 (2008).
15. G. Zhou, L. Zhang, F. Li, X. Hu, T. Wang, Q. Li, M. Qiu, and Y. Su, "All-optical temporal differentiation of ultra-high-speed picosecond pulses based on compact silicon microring resonator," Electron. Lett. **47**(14), 814–816 (2011).
16. C. Cuadrado-Laborde and M. V. Andrés, "In-fiber all-optical fractional differentiator," Opt. Lett. **34**(6), 833–835 (2009).
17. M. Li, L.-Y. Shao, J. Albert, and J. Yao, "Continuously tunable photonic fractional temporal differentiator based on a tilted fiber Bragg grating," IEEE Photon. Technol. Lett. **23**(4), 251–253 (2011).
18. H. Shahoei, J. Albert, and J. Yao, "Tunable fractional order temporal differentiator by optically pumping a tilted fiber Bragg grating," IEEE Photon. Technol. Lett. **24**(9), 730–732 (2012).
19. H. Shahoei, D.-X. Xu, J. H. Schmid, and J. Yao, "Photonic fractional-order differentiator using an SOI microring resonator with an MMI coupler," IEEE Photon. Technol. Lett. **25**(15), 1408–1411 (2013).
20. A. Zheng, J. Dong, L. Zhou, X. Xiao, Q. Yang, X. Zhang, and J. Chen, "Fractional-order photonic differentiator using an on-chip microring resonator," Opt. Lett. **39**(21), 6355–6358 (2014).
21. A. Zheng, T. Yang, X. Xiao, Q. Yang, X. Zhang, and J. Dong, "Tunable fractional-order differentiator using an electrically tuned silicon-on-isolator Mach-Zehnder interferometer," Opt. Express **22**(15), 18232–18237 (2014).
22. D. R. Solli, P. Koonath, and B. Jalali, "Inverse Raman scattering in silicon: a free-carrier enhanced effect," Phys. Rev. A **79**(5), 053853 (2009).
23. Y. Xiong and W. N. Ye, "All-optical switching of a single wavelength in a silicon-based ring-assisted Mach-Zehnder interferometer," Appl. Opt. **51**(32), 7788–7793 (2012).
24. Y. H. Wen, O. Kuzucu, T. Hou, M. Lipson, and A. L. Gaeta, "All-optical switching of a single resonance in silicon ring resonators," Opt. Lett. **36**(8), 1413–1415 (2011).
25. Y. H. Wen, O. Kuzucu, M. Fridman, A. L. Gaeta, L.-W. Luo, and M. Lipson, "All-optical control of an individual resonance in a silicon microresonator," Phys. Rev. Lett. **108**(22), 223907 (2012).
26. W. Bogaerts, P. De Heyn, T. Van Vaerenbergh, K. De Vos, S. Kumar Selvaraja, T. Claes, P. Dumon, P. Bienstman, D. Van Thourhout, and R. Baets, "Silicon microring resonators," Laser Photonics Rev. **6**(1), 47–73 (2012).
27. S. Feng, T. Lei, H. Chen, H. Cai, X. Luo, and A. Poon, "Silicon photonics: from a microresonator perspective," Laser Photonics Rev. **6**(2), 145–177 (2012).
28. J. E. Heebner, V. Wong, A. Schweinsberg, R. W. Boyd, and D. J. Jackson, "Optical transmission characteristics of fiber ring resonators," IEEE J. Quantum Electron. **40**(6), 726–730 (2004).
29. M. Krause, H. Renner, and E. Brinkmeyer, "Silicon Raman amplifiers with ring-resonator-enhanced pump power," IEEE J. Sel. Top. Quantum Electron. **16**(1), 216–225 (2010).
30. I. D. Rukhlenko, M. Premaratne, and G. P. Agrawal, "Nonlinear silicon photonics: analytical tools," IEEE J. Sel. Top. Quantum Electron. **16**(1), 200–215 (2010).
31. Q. Lin, O. J. Painter, and G. P. Agrawal, "Nonlinear optical phenomena in silicon waveguides: Modeling and applications," Opt. Express **15**(25), 16604–16644 (2007).
32. X. Sang and O. Boyraz, "Gain and noise characteristics of high-bit-rate silicon parametric amplifiers," Opt. Express **16**(17), 13122–13132 (2008).
33. A. C. Turner-Foster, M. A. Foster, J. S. Levy, C. B. Poitras, R. Salem, A. L. Gaeta, and M. Lipson, "Ultrashort free-carrier lifetime in low-loss silicon nanowaveguides," Opt. Express **18**(4), 3582–3591 (2010).
34. Y. Vlasov and S. McNab, "Losses in single-mode silicon-on-insulator strip waveguides and bends," Opt. Express **12**(8), 1622–1631 (2004).

1. Introduction

With the rapid development of high-speed optical communication networks, all-optical signal processing technology is an effect approach to overcome the inherent speed limitations of conventional electronics. The temporal photonic differentiator is a basic element which can implement the time derivative of the complex envelope of the input optical pulse. It can be used in a wide range of applications, such as ultrafast all-optical computing [1], pulse shaping and coding [2–4], dark-soliton detection [5], and Hermite-Gaussian waveforms generation [6]. Different schemes have been proposed to realize the temporal differentiation based on the interferometers, fiber gratings, programmable pulse shapers, photonic crystal nanocavities, and microring resonators [7–13]. In particular, the silicon based microring resonator has been considered as a promising scheme with the advantages of compactness, mature fabrication, and photonic-electronic integration [12–15].

In addition to the regular integer-order temporal differentiator, the fractional-order differentiator has also attracted considerable research interest [16–21]. It has been recently demonstrated that the fractional-order differentiation can be implemented by using the under-coupled and over-coupled microring resonators [19,20]. However, the differentiation order

#233705 - $15.00 USD Received 3 Feb 2015; revised 15 Apr 2015; accepted 16 Apr 2015; published 21 Apr 2015

can only be tuned electrically in the scheme reported in [20], which limits the response speed. In [19], the differentiation order is controlled by the polarization state of the input light-wave. As the polarization convertor and the multimode interference (MMI) coupler are required in this scheme, the device complexity is increased.

In the inverse Raman scattering (IRS) process, light at the anti-Stokes wavelength is strongly attenuated in the presence of an intense pump [22]. In silicon, IRS has already been used for wavelength-selective all-optical switching, where the intracavity loss of an optical resonator is precisely controlled in real time [23–25]. In this paper, a novel fractional-order temporal differentiator is proposed in a microring resonator on the silicon-on-insulator (SOI) platform. The coupling coefficient of the resonator is kept constant, while the intracavity loss is adjusted by the pump intensity using the IRS effect. Thus, the continually tunable differentiation order can be realized. By increasing the pump power continuously from 60 mW to 95 mW, the Gaussian pulse with a full width at half-maximum (FWHM) of 50 ps can be differentiated with the order from 1.6 to 0.3, and the output deviation from an ideal fractional-order differentiator is maintained less than 5%. Due to the narrow bandwidth of IRS in silicon, the adjustment of intracavity loss can be implemented on a specific resonance while leaving the adjacent resonances undisturbed. As a result, the proposed scheme has the potential to achieve different differentiation orders simultaneously at different resonant wavelengths. Furthermore, the effects of input pulse width on the differentiation order and the average deviation are discussed in detail, which have not been analyzed in previous literatures on the microring-based fractional-order differentiators.

2. Operational principle

For an input signal $x(t)$, the n th-order differentiator with an output $dx^n(t)/dt^n$ can be considered as an optical filter. The transfer function $H_n(\nu)$ is given by [16,18]:

$$\begin{aligned} H_n(\nu) &= (i2\pi\nu)^n \\ &= \begin{cases} |2\pi\nu|^n \exp(in\pi/2) & \nu > 0 \\ |2\pi\nu|^n \exp(-in\pi/2) & \nu < 0 \end{cases}, \end{aligned} \tag{1}$$

where $n \in \mathbb{R}^+$, $\nu = (\omega - \omega_0)/2\pi$ is the baseband frequency, ω is the optical frequency, and ω_0 is the carrier frequency. It can be seen that the amplitude response is $|2\pi\nu|^n$, and the phase response has a phase shift of $n\pi$ across ω_0. The transfer function can be approximately implemented using the all-pass microring resonator, as illustrated in Fig. 1. The intensity transmission T and the phase response Φ of an all-pass microring resonator are given by [26–28]:

$$T = \left|\frac{E_2}{E_1}\right|^2 = \frac{\tau^2 - 2r\tau\cos\phi + r^2}{1 - 2r\tau\cos\phi + r^2\tau^2}, \tag{2}$$

$$\begin{aligned} \Phi &= \arg\left(\frac{E_2}{E_1}\right) \\ &= \pi + \phi + \arctan\left(\frac{r\sin\phi}{\tau - r\cos\phi}\right) + \arctan\left(\frac{r\tau\sin\phi}{1 - r\tau\cos\phi}\right), \end{aligned} \tag{3}$$

where r is the transmission coefficient of the coupling region, $\phi = \beta L$ is the round-trip phase shift with the circumference L and the propagation constant β, and $\tau = \exp(-\alpha(\omega)L/2)$ is the round-trip amplitude transmission with the power loss coefficient α. As shown in Fig. 2, the critical-coupled microring, where $r = \tau$, can provide a phase shift

#233705 - $15.00 USD Received 3 Feb 2015; revised 15 Apr 2015; accepted 16 Apr 2015; published 21 Apr 2015

of π across the resonance. Therefore, when the wavelength of input optical pulse coincides with one of the resonance, a microring resonator operating at the critical coupling condition can be used as a first-order differentiator. In addition, as the phase shifts of smaller and greater than π can be achieved when $r > \tau$ and $r < \tau$ are satisfied respectively, the fractional-order differentiator with $0 < n < 2$ can be implemented using the under-coupled and the over-coupled microring resonators.

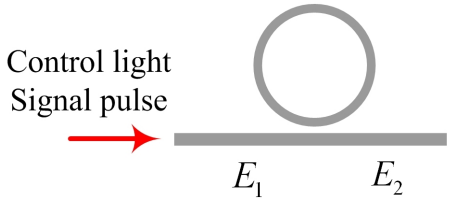

Fig. 1. Schematic illustration of the fractional-order temporal differentiator realized by the IRS effect in the side-coupled microring resonator.

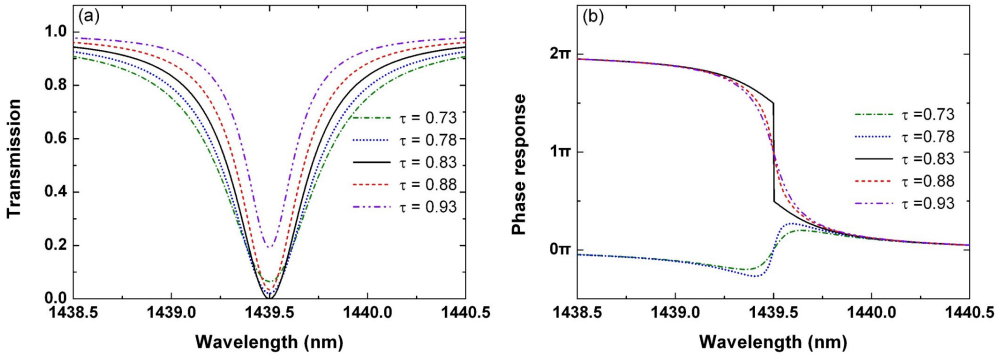

Fig. 2. (a) Intensity transmission and (b) phase response for the microring resonator with $r = 0.83$ and varying values of τ.

In the IRS process, anti-Stokes photons are transferred to the pump, which leads to an attenuation of the anti-Stokes light-wave. In silicon, the anti-Stokes wavelength is blue-shifted by 15.6 THz with respect to the pump wavelength, and the bandwidth of spectral loss is 105 GHz [22,25]. The IRS process is governed by the generalized nonlinear Schrödinger equation (NLSE) in [22]. However, the loss coefficient α_R induced by IRS near the anti-Stokes frequency ω_a can be simplified and described as [25]:

$$\alpha_R(\omega, I) = \frac{g_R \Gamma_R^2}{(\omega - \omega_a)^2 / 4\pi^2 + \Gamma_R^2} I, \tag{4}$$

where $\Gamma_R = 105$ GHz, I is the pump intensity, and $g_R = 7$ cm/GW is the Raman gain coefficient when the pump wavelength is 1550 nm. In our scheme illustrated in Fig. 1, the radius of the microring is optimized so that both the pump and the signal wavelengths are on resonance. Due to the field enhancement effect at the resonant wavelengths, the pump intensity is much larger in the ring than that in the straight waveguide. Thus, the IRS process only occurs in the resonator, and can be neglected outside the ring. The intracavity intensity can be calculated by $I = MP_{pi} / A_{eff}$, where P_{pi} is the input pump power, A_{eff} is the effective mode area of the pump, and $M = (1 - r^2) / (1 - r\tau)^2$ is the power enhancement factor at the pump wavelength [29,30].

#233705 - $15.00 USD Received 3 Feb 2015; revised 15 Apr 2015; accepted 16 Apr 2015; published 21 Apr 2015

In the absence of the pump light-wave, as the signal power is rather small, the power loss in the microring resonator is mainly caused by the linear loss of the bended waveguide, i.e. $\alpha = \alpha_L$. However, when the pump and the signal light-waves are launched into the waveguide simultaneously, the intense pump light-wave will result in the nonlinear processes, such as the Kerr effect, IRS, two-photon absorption (TPA), free carrier absorption (FCA), and free carrier dispersion (FCD). Beside IRS, TPA and FCA lead to an additional attenuation of the signal light-wave, while the Kerr effect and FCD cause a change of the refractive index [31]. Therefore, the power loss coefficient at the signal wavelength in the microring resonator can be written as $\alpha = \alpha_L + \alpha_R + \alpha_T + \alpha_F$, where α_L is the linear loss coefficient, $\alpha_T = 2\beta_{TPA} I$ and α_F are caused by TPA and FCA respectively, and $\beta_{TPA} = 0.45$ cm/GW is the TPA coefficient. In addition, the FCA loss coefficient can be calculated by $\alpha_F = 1.45 \times 10^{-21} (\lambda_s / \lambda_{ref})^2 N$, where $\lambda_{ref} = 1550$ nm, λ_s is the signal wavelength, the free carrier density N obeys the rate equation $\partial N / \partial t = \beta_{TPA} I^2 / (2\hbar\omega_p) - N / \tau_0$, and τ_0 is the effective carrier lifetime [31,32]. By adopting the reverse-biased p-i-n structures, the free carrier lifetime can be decreased significantly, so that FCA and FCD are both reduced [33]. The refractive index change induced by FCD can be cancelled out by the Kerr effect, so the resonant wavelength is kept constant [23–25].

3. Results and discussion

In this work, the silicon waveguides have a cross section of 450 nm × 250 nm. The TE polarized pump and the TM polarized signal are launched at 1556.1 nm and 1439.5 nm, respectively. The TE-TM pump-signal combination can reduce the difference of coupling coefficients at the two wavelengths, while increase the Raman induced loss by a factor of 1.5 [25]. A microring with the radius $R = 50$ μm is used, so both the pump and the signal are on resonance. In the absence of the pump, the microring resonator is over-coupled at the signal wavelength with $\alpha_L = 10.77$ dB/cm and $r = 0.83$. As the coupling strength and the linear loss coefficient are related to the wavelength and the polarization state, the resonator is operated near the critical coupling condition at the pump wavelength with $\alpha_L = 5$ dB/cm and $r = 0.97$ [25,34]. The free carrier lifetime is $\tau_0 = 50$ ps.

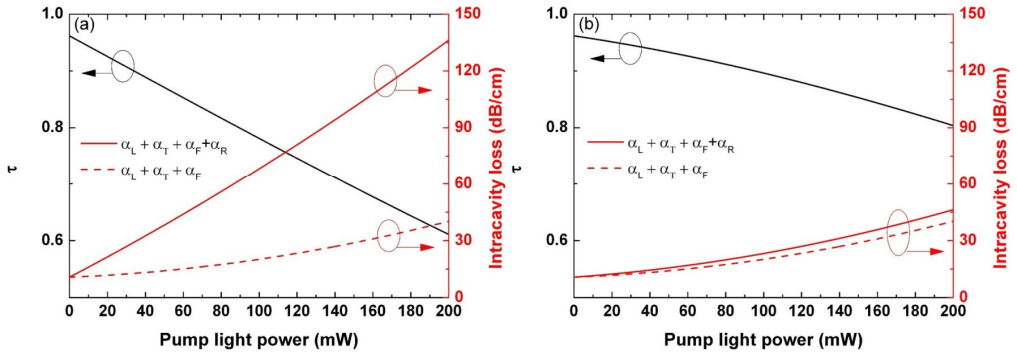

Fig. 3. τ and intracavity loss at (a) 1439.5 nm and (b) 1442.3 nm as functions of the pump light power. The dashed lines depict the intracavity loss induced by all the mechanisms except IRS, and the solid lines include all the optical losses in the resonator.

Figure 2 shows the power transmission and the phase response of the microring resonator. When the difference between r and τ is increased, the slope of phase response across the resonance and the resonant attenuation are both decreased. Moreover, the 3-dB bandwidth of the transmission spectrum is increased with the decrease of τ .

#233705 - $15.00 USD Received 3 Feb 2015; revised 15 Apr 2015; accepted 16 Apr 2015; published 21 Apr 2015

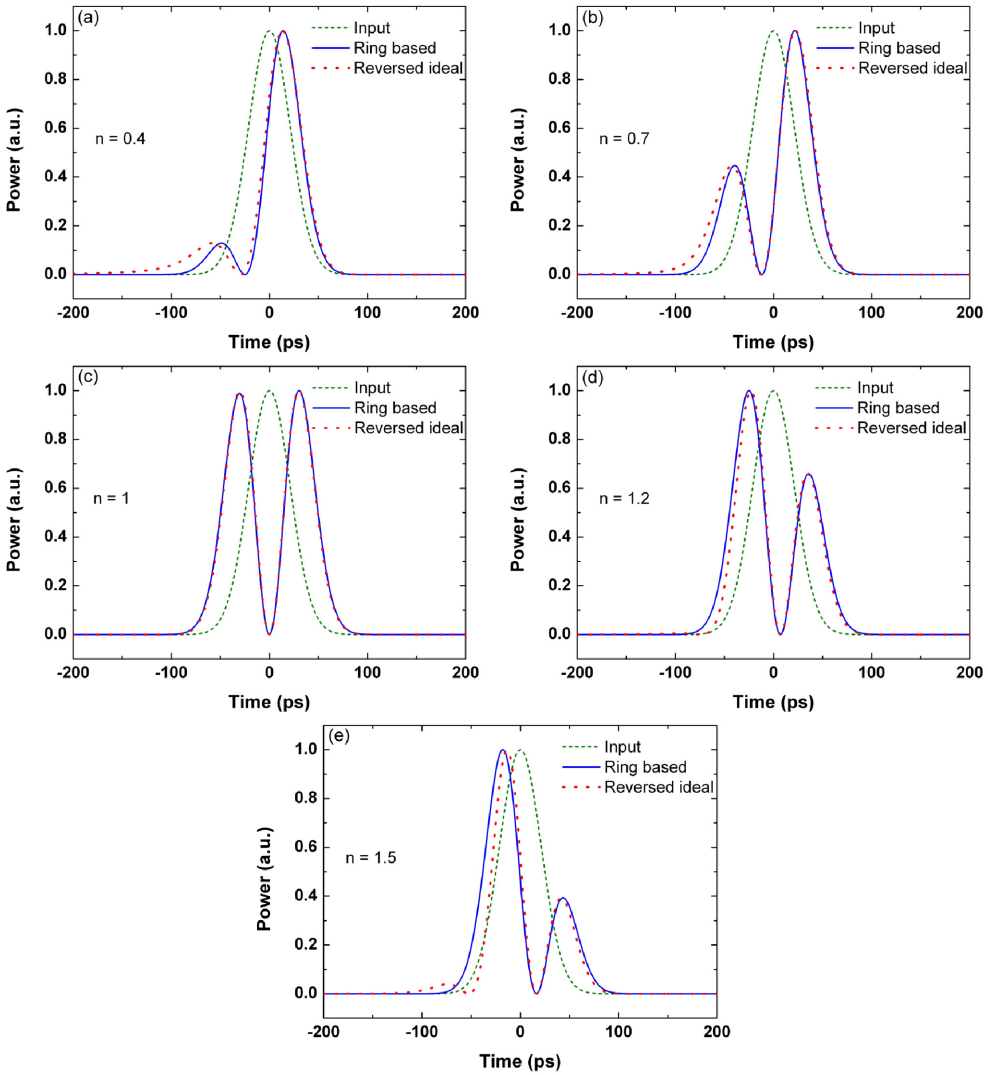

Fig. 4. Comparisons between the outputs of the proposed differentiator and the time-reversed ideal differentiator with (a) $n = 0.4$, (b) $n = 0.7$, (c) $n = 1$, (d) $n = 1.2$, and (e) $n = 1.5$. The FWHM of the input Gaussian pulse is 50 ps.

As mentioned above, for the continuous-wave pump, α_R and α_F are proportional to I and I^2 respectively, and α_T is much smaller than α_R. When the pump light-wave is injected into the resonator, as shown in Fig. 3(a), the intracavity loss at the signal wavelength is nearly linear with respect to the pump power, which indicates the signal attenuation is predominated by the IRS effect. With the increase of the pump power, the round-trip amplitude transmission coefficient τ is decreased, and the coupling state at the signal wavelength will be altered from the over-coupled regime to the critical-coupled regime, and then to the under-coupled regime.

The effect of pump light-wave on the intracavity loss at 1442.3 nm is shown in Fig. 3(b), where 1442.3 nm is the resonance adjacent to the anti-Stokes wavelength. The bandwidth of IRS is much smaller than the free spectral range (FSR) of the microring resonator. Therefore, the optical loss induced by IRS is decreased significantly compared with that at the anti-Stokes wavelength. The optical loss induced by TPA and FCA is kept almost constant within

#233705 - $15.00 USD Received 3 Feb 2015; revised 15 Apr 2015; accepted 16 Apr 2015; published 21 Apr 2015

the FSR. Thus, for the resonances which do not coincide with the anti-Stokes wavelength, it can be seen that TPA and FCA plays an important role in the intracavity loss.

When a Gaussian pulse with a temporal FWHM of 50 ps is launched into the resonator as the signal, by properly adjusting the pump power, differentiated pulses with the order n = 0.4, 0.7, 1, 1.2, and 1.5 can be generated as shown in Fig. 4. Compared with the outputs of the time-reversed ideal differentiators, it can be seen that the waveform deviation is relevant to the differentiation order n. A good agreement can be observed when the differentiation order is close to 1. In addition, the waveform deviation with $n>1$ is greater than that with $n<1$. The dependence of waveform deviation on the differentiation order will be further discussed in the later part of this section.

The effect of pump power on the differentiation order is described in Fig. 5. When the pump power is varied from 60 mW to 95 mW, the input pulse with FWHM = 50 ps can be differentiated with the order from 1.6 to 0.3. There is approximately a linear correlation between the pump power and the differentiation order with $n>1$. When $n<1$, the differentiation order is decreased more and more slowly with the increase of the pump power. Besides, under the critical coupling condition where $r=\tau=0.83$, the differentiation order is equal to $n=1$ for all the input signal pulses with FWHM ≥ 50 ps. However, a small discrepancy from the differentiation order $n=1$ can be observed for the input pulse with FWHM = 20 ps.

The differentiation order is also affected by the pulse width of the input signal light-wave. The input with larger pulse width has less bandwidth in its spectrum. If the input spectrum is concentrated more densely to one of the resonances, the output will be more sensitive to the change of resonator response which is induced by the variation of τ. Therefore, when the input pulse width is increased, the curve in Fig. 5 becomes steeper indicating the differentiation order is more sensitive to the pump power. In practical applications, we can increase the input pulse width to reduce the required variation range of the pump power. On the contrary, decreasing the input pulse width is beneficial to improve the tuning accuracy of the differentiation order.

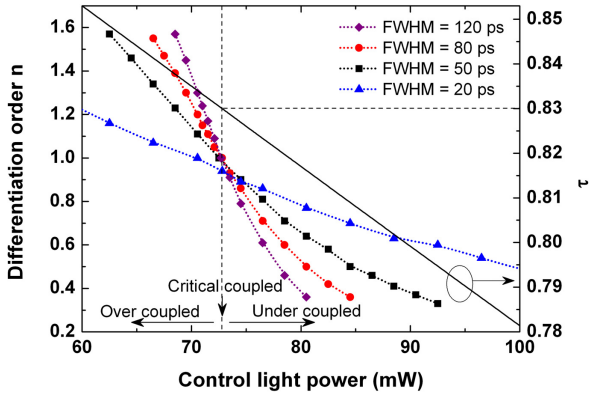

Fig. 5. Differentiation order as function of the pump power and the input pulse width. To indicate the coupling state of the microring resonator, the correspondence of the pump power and the round-trip amplitude transmission coefficient is also presented.

As seen from Fig. 5, one pump power can correspond to more than one differentiation orders due to the variation of the input pulse width. This phenomenon can be attributed to two factors. One is the insufficient bandwidth of the microring resonator. Figure 6(a) shows the output under the critical coupling condition for various input pulse widths. A discrepancy from the first-order differentiator can be observed for the input pulse with FWHM = 20 ps, where the two peaks of the output have different maximums. In fact, the output can be fitted using an ideal fractional-order differentiator with $n=0.94$. It is noteworthy that this

#233705 - $15.00 USD Received 3 Feb 2015; revised 15 Apr 2015; accepted 16 Apr 2015; published 21 Apr 2015

discrepancy will not emerge when the input pulse width exceeds FWHM = 50 ps. On the resonance, the critical-coupled microring resonator is quite ideal for the first-order differentiator, as the transmission is completely repressed and the phase is shifted by exact π radians with almost infinite slope. Hence, it can be deduced that the discrepancy in Fig. 6(a) is derived from the insufficient bandwidth of the resonator. The bandwidth can be increased by decreasing R and r, while greater pump power will be required to achieve the same differentiation order. The second factor is the response of the over-coupled and under-coupled microring resonator does not perfectly coincide with that of an ideal fractional-order differentiator. The transmission of the resonator cannot be attenuated to 0 on the resonance. Furthermore, the phase response is more crucial where the slope of the phase shift across the resonance declines with the increase of $|r-\tau|$. In Fig. 6(b), the differentiation orders with $\tau = 0.834$ are $n = 1.11$ and $n = 1.2$ for the input pulses with FWHM = 50 ps and FWHM = 80 ps, respectively. When $\tau = 0.816$, the differentiation orders are $n = 0.64$ and $n = 0.5$ for these pulse widths as shown in Fig. 6(c). The differentiation orders for the input pulse with FWHM = 20 ps are $n = 1$ and $n = 0.77$ in Fig. 6(b) and Fig. 6(c) respectively, which are affected by both of the two factors simultaneously.

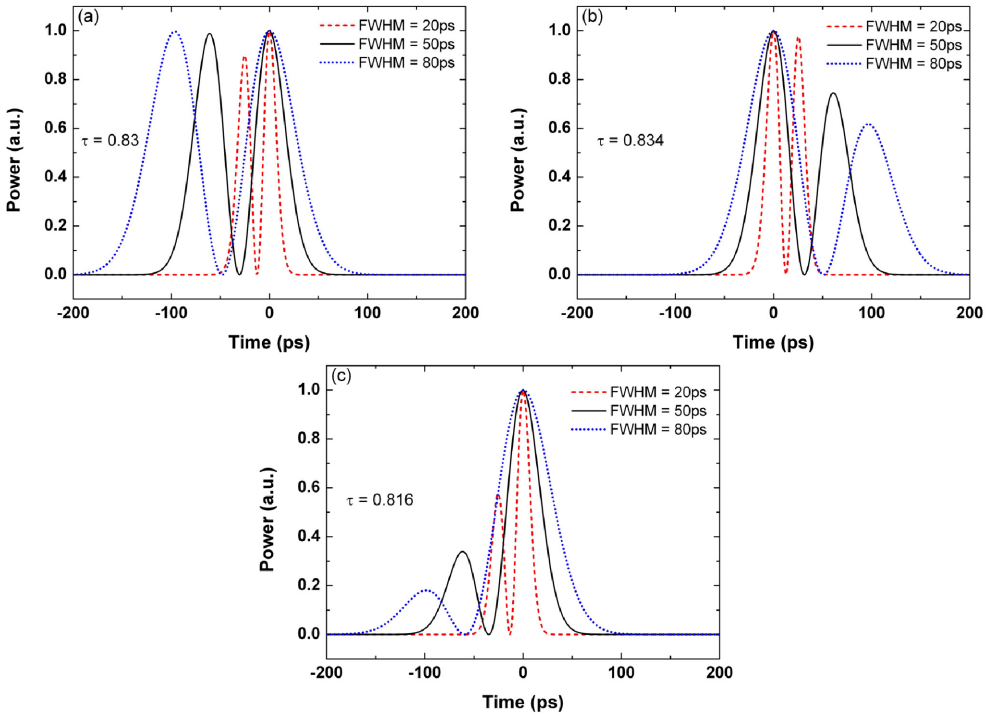

Fig. 6. Output of the proposed differentiator for various input pulse widths with (a) $\tau = 0.834$, (b) $\tau = 0.83$, and (c) $\tau = 0.816$.

To quantitatively evaluate the performance of the proposed fractional-order differentiator, the average deviation D_{ave} can be defined as the mean absolute deviation between the outputs of the ideal and the microring-based differentiators [8]:

$$D_{ave} = \frac{1}{T}\int_{T} \left| P_{MR}(t) - P_i(t) \right| dt, \tag{5}$$

#233705 - $15.00 USD Received 3 Feb 2015; revised 15 Apr 2015; accepted 16 Apr 2015; published 21 Apr 2015

where $P_{MR}(t)$ and $P_i(t)$ are both normalized output powers. In this work, to guarantee the successive output pulses do not overlap with each other, the time repetition period of the input waveform is $T = 6 \times FWHM$, where FWHM is the input pulse width.

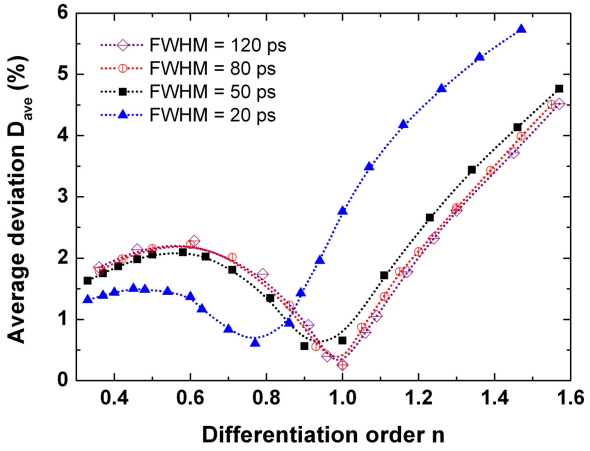

Fig. 7. Effects of the differentiation order and the input pulse width on the average deviation in the proposed differentiator.

The average deviation of the proposed differentiator for various input pulse widths is presented in Fig. 7. To demonstrate the effect of differentiation order on the average deviation, we focus on the curve for the input FWHM = 80 ps, where the bandwidth of the microring resonator is sufficient for the input pulse. As discussed before, the critical-coupled microring resonator has the most similar spectral response compared to the ideal differentiator, so the average deviation has a minimum at $n = 1$. With the differentiation order departing from 1, the spectral response of the resonator deteriorates more and more seriously from the ideal fractional-order differentiator, so the average deviation is increased. Quite interestingly, the average deviation has a local maximum near $n = 0.6$. As seen from Fig. 4(a) and Fig. 4(b), when $n < 1$, the deviation is mainly derived from the minor peak of the output, while the minor peak of output pulse for the ideal differentiator declines with the decrease of n . The discrepancy of spectral response promotes the growth of the deviation, and on the contrary, the declining of the minor peak of output diminishes the average deviation. Thus, the two effects counteract with each other, and form the local maximum of the average deviation. However, when $n > 1$, the average deviation is monotonous with respect to the differentiation order n .

Figure 7 also depicts the effect of input pulse width on the average deviation. With the decrease of the input FWHM, the minimum of the deviation curve is increased, while the differentiation order corresponding to the minimum deviation is reduced. In addition, although less deviation can be obtained for small differentiation orders, the deviation with $n > 1$ will be increased. Hence, there is a trade-off for the deviations with small and large differentiation orders. For the input FWHM ≥ 50 ps where sufficient bandwidth can be provided by the microring resonator, the curve shift caused by the input pulse width is inconspicuous. It can be seen that the deviation curves for input FWHM = 80 ps and FWHM = 120 ps are almost coincident with each other. In this case, compared to Fig. 5, although the required pump power is varied with the input pulse width to achieve a particular differentiation order n , the average deviation D_{ave} can be held relatively constant.

#233705 - $15.00 USD Received 3 Feb 2015; revised 15 Apr 2015; accepted 16 Apr 2015; published 21 Apr 2015

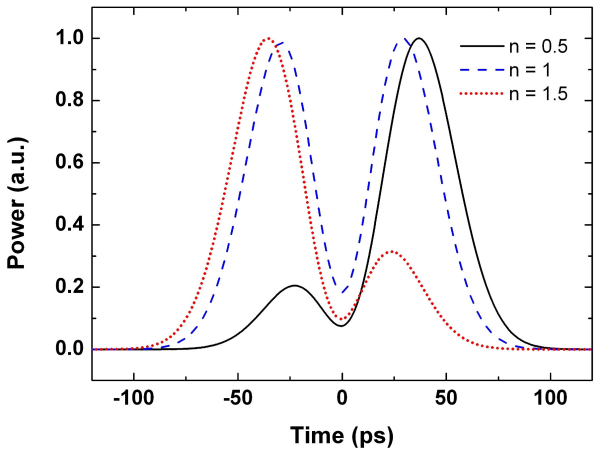

Fig. 8. Output of the proposed differentiator when the signal wavelength is shifted to 1439.51 nm. The differentiation order is $n = 0.5$, $n = 1$, and $n = 1.5$, respectively.

As discussed before, in the microring-based differentiator, the signal wavelength should coincide with one of the resonant wavelengths. However, the resonant wavelengths can be shifted by many factors, such as the light intensity, the free carrier density, and the thermal effect. To analyze the effect of resonance shift on the output waveform, without loss of generality, we assume the resonant wavelength is kept at 1439.5 nm, and the anti-Stokes signal pulses are launched at 1439.51 nm. The differentiated pulses with $n = 0.5$, $n = 1$, and $n = 1.5$ are depicted in Fig. 8. When the signal is detuned from the resonance, it can be seen that the optical power cannot drop to zero in the notch part of the output waveform. Therefore, to reduce the output deviation of the microring-based differentiator, it is crucial to decrease the mismatch between the signal and the resonant wavelength.

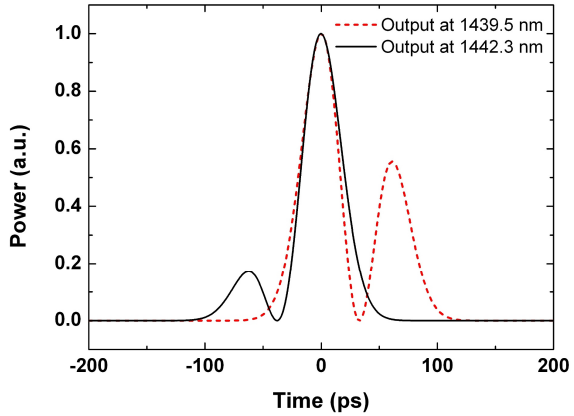

Fig. 9. The 1.23-order differentiated pulse at 1439.5 nm and the 0.49-order differentiated pulse at 1442.3 nm, where the 50 mW and 70 mW pump light-waves are launched at 1556.1 nm and 1559.2 nm simultaneously. The FWHM of the input Gaussian pulses is 50 ps.

As shown in Fig. 3(b), due to the narrow bandwidth of IRS, the intracavity loss induced by IRS is rather small except for the anti-Stokes resonance. Thus, different differentiation orders can be realized simultaneously at different resonant wavelengths by launching multiple pump light-waves. For instance, two pump light-waves at $\lambda_{P1} = 1556.1$ nm and $\lambda_{P2} = 1559.2$ nm are injected into the resonator with the power $P_{P1} = 50$ mW and $P_{P2} = 70$ mW. As shown in Fig. 9, when the Gaussian pulses with FWHM = 50 ps are launched as the anti-Stokes input

#233705 - $15.00 USD Received 3 Feb 2015; revised 15 Apr 2015; accepted 16 Apr 2015; published 21 Apr 2015

signals, the 1.23-order differentiated pulse can be obtained at 1439.5 nm with the average deviation $D_{ave} = 2.7\%$, and at the same time, the 0.49-order differentiated pulse can be obtained at 1442.3 nm with $D_{ave} = 2.0\%$. The TPA process occurs between the signal and each pump light-wave, and the free carrier is generated by both of the pump light-waves. Therefore, compared with the signal-pump configuration with $P_{P1} = 50$ mW or $P_{P2} = 70$ mW, the intracavity loss is increased and the differentiation order is decreased. Besides, the four-wave mixing (FWM) effect is negligible, as the signal wavelengths are far from its gain-bandwidth.

4. Conclusion

In summary, using the IRS effect in silicon waveguide, a novel photonic fractional-order temporal differentiator is proposed based on the side-coupled microng resonator. By controlling the power of the pump light-wave, the intracavity loss is adjusted, and the coupling state of the microring resonator can be changed. Thus, the differentiation order can be tuned continuously. As the microring resonator has limited bandwidth and non-ideal spectral response as a fractional-order differentiator, the required pump power is varied with the input pulse width to obtain a particular differentiation order. In addition, with the increase of the input pulse width, the differentiation order becomes more sensitive to the variation of pump power. Compared with the output of an ideal fractional-order differentiator, the average deviation is minimal when the differentiation order is close to 1. The average deviation is monotonous with respect to the differentiation order when $n > 1$, while it has a local maximum when $n < 1$. While altering the input pulse width, the correspondence between the average deviation and the differentiation order is shifted, and there is a trade-off for the deviations with small and large differentiation orders. However, the shift is inconspicuous when sufficient bandwidth can be provided by the microring resonator. The proposed scheme offers a new approach to realize the optically tunable fractional-order differentiation in the microring resonator. The narrow attenuation bandwidth of the IRS process in silicon provides the potential to achieve different differentiation orders simultaneously at different resonant wavelengths. Furthermore, this work has discussed the influencing factors on the differentiation order and the average deviation, which can be applied to all the fractional-order differentiators based on microring resonators.

Acknowledgments

This work is partly supported by the National Natural Science Foundation of China (61307109 and 61475023), the Natural Science Foundation of Beijing (4152037), the National High-Technology Research and Development Program of China (2013AA031501), the Specialized Research Fund for the Doctoral Program of Higher Education (20120005120021), the Fundamental Research Funds for the Central Universities (2013RC1202), the China Postdoctoral Science Foundations (2012M511826 and 2014M552213), the Fund of State Key Laboratory of Information Photonics and Optical Communications (Beijing University of Posts and Telecommunications) P. R. China, the Hong Kong Scholars Program 2013 (PolyU G-YZ45), the Research Grant Council of the Hong Kong Special Administrative Region China (PolyU5272/12E), and the Science Foundation Ireland (SFI) under the International Strategic Cooperation Award Grant Number SFI/13/ISCA/2845.

#233705 - $15.00 USD Received 3 Feb 2015; revised 15 Apr 2015; accepted 16 Apr 2015; published 21 Apr 2015